International Journal of Biological Macromolecules 175 (2021) 217–228

Contents lists available at ScienceDirect

International Journal of Biological Macromolecules

journal homepage: http://www.elsevier.com/locate/ijbiomac

Preparation and evaluation of functional allopurinol imprinted starch based biomaterials for transdermal drug delivery

Han-Seong Kim [a,1], Yeon-Hum Yun [b,1], Wang-Geun Shim [c,*], Soon-Do Yoon [a,*]

[a] Department of Chemical and Biomolecular Engineering, Chonnam National University, Yeosu 59626, Republic of Korea
[b] Geoconvergence Research Center, Chonnam National University, Gwangju 61186, Republic of Korea
[c] Department of Polymer Science and Engineering, Sunchon National University, Suncheon, Jeollanam-do 57922, Republic of Korea

ARTICLE INFO

Article history:
Received 19 November 2020
Received in revised form 15 January 2021
Accepted 1 February 2021
Available online 4 February 2021

Keywords:
Functional starch-based biomaterials
Allopurinol
Recognition properties
Drug release behavior
Thermo-sensitive properties

ABSTRACT

This study focuses on the synthesis of functional allopurinol (ALP) imprinted biomaterials for a transdermal drug delivery using mung bean starch (MBS), polyvinyl alcohol (PVA), sodium benzoate (SB) as a crosslinking agent, and poloxamer (PX) as a thermo-sensitive polymer. Prepared functional biomaterials were characterized and evaluated by SEM, FT-IR analysis, and physical properties. Results of ALP recognition properties indicated that adsorbed amounts (Q) of ALP on functional ALP imprinted biomaterials were 3.8 to 4.9-fold higher than that of non-ALP imprinted biomaterial. Results of ALP release revealed that the ALP release rate for PX added biomaterials was 1.10 (36.5 °C) or 1.30 (45 °C) times faster than that at 25 °C. These results indicate that functional ALP imprinted biomaterials have thermo-sensitive properties due to the addition of PX. Results of ALP release using artificial skin indicated that ALP release was increased at a relatively steady-state rate for 3 h and that the ALP release behavior followed the non-Fickian diffusion mechanism.

1. Introduction

Gout is a common inflammatory disease with a prevalence of about 1% in Western society. Gout is a disease in which uric acid crystals are accumulated in tissues such as cartilage and tendons in joints due to the formation of uric acid in the blood. These deposited crystals can lead to serious inflammation with extreme pain to patients [1–5]. Gout disease is generally treated using nonsteroidal anti-inflammatory drugs or systemic glucocorticoids to lower uric acid levels in the blood. Allopurinol (ALP) is known to inhibit the production of uric acid by inhibiting xanthine oxidase involved in the oxidation of hypoxanthine and xanthine. However, side effects such as allopurinol hypersensitivity syndrome and kidney damage may occur when a high dosage is used. Therefore, many studies have investigated effective drug delivery with minimal of side effects for drug treatment [6,7].

A transdermal drug delivery system (TDDS) can deliver drugs directly to the local area, minimizing the problem of systemic toxicity of conventional drug treatment (e.g. oral or injection administration) and increasing effective drug concentration at the lesion site. In particular, a non-invasive technique of delivering drugs through the skin has many advantages such as painlessness, easiness for self-administration, flexibility in dosage regimen, convenience, and high patient compliance. However, the penetration effect of a drug is reduced because the stratum corneum outside the skin has a protective action. In addition, a small molecule drug with high hydrophilicity has a disadvantage in that it can be absorbed through the stratum corneum. Therefore, it is necessary to solve the impermeability problem of the skin and develop a transdermal drug delivery system that is capable of letting various drugs to permeate the skin as an effective treatment strategy [8–11].

Recently, a functional patch using a stimulus-responsive polymer or microneedle to enhance the permeability of a drug has emerged as an attractive candidate for biomedical applications. Among stimulus-responsive polymers, a thermo-sensitive polymer generally has a balance between a hydrophobic group and a hydrophilic group with a low critical solution temperature (LCST) that can cause the polymer chain to contract and swell according to a temperature change [12,13]. Poloxamer 407 (PX) with LCST properties near body temperature as a temperature-sensitive polymer is a block copolymer composed of poly (ethylene oxide) and poly(propyl oxide). It is widely used in controlled release drug delivery systems based on sol-gel phase transition [14,15].

Good biocompatibility and biodegradability are essential conditions of biomedical materials for in vivo applications. Currently used biomedical materials for transdermal drug delivery patches include poly(vinyl alcohol), polyacrylamide, poly(ethylene glycol), polylactides, polyglycolides, poly(lactide-co-glycolides), proteins (albumin, collagen, β-casein, gelatin, silk, and zein), and carbohydrates (alginate, chitosan,

* Corresponding authors.
E-mail addresses: wgshim@sunchon.ac.kr (W.-G. Shim), yunsd03@jnu.ac.kr (S.-D. Yoon).
[1] These authors contributed equally to this work.

https://doi.org/10.1016/j.ijbiomac.2021.02.004
0141-8130/

heparin, pululan, and starch). Of these biomedical materials, petroleum-based polymers or synthetic polymers have some drawbacks such as low biodegradability in landfills and soil, human side-effects, and environment pollutions though they are biocompatibility, durability, and convenience. Therefore, an investigations and studies have been conducted to develop and examine replacement biomaterials based on biodegradable polymers such as starch, chitosan, cellulose, alginate, gelatin, inulin, and so on. Starch is one type of carbohydrates. It has excellent biocompatibility and biodegradability with a low cost. However, its physical properties are worse than those of synthetic polymers [16–18]. To overcome this limitation, various crosslinking methods have been used for starch-based biomedical materials such as adding functional additives, using chemical crosslinking agents, utilizing nanoparticles, performing heat treatment, and using electron bean irradiation [19].

In our previous study, we have prepared UV cured starch-based biomaterials imprinted with sulindac [20] and atenolol [21] for a transdermal drug delivery system and reported their application. Experimental results have validated that their physical properties are improved using UV curing process. In addition, we confirmed the possible application of sulindac or atenolol imprinted starch-based biomaterials as transdermal drug delivery patches. Although many studies have been reported various functional transdermal drug delivery patches using biomedical materials with good biocompatibility and biodegradability, few studies have performed on PX or press needles for the improvement of functionality in a transdermal drug delivery patch. Herein, in order to improve effective drug release and treat patients with acute gout, ALP imprinted biomaterials added with PX as a thermo-sensitive polymer. Press needles commonly used in oriental medicine were also used for preparing transdermal drug delivery patches.

The main objective of this study was to prepare functional thermo-sensitive ALP imprinted biomaterials added with PX. Their physical properties, recognition properties of ALP for quantitative analysis, and ALP release behavior under different pH and temperature conditions were then investigated. ALP recognition and ALP release mechanism were evaluated using well-known adsorption isotherms (Langmuir, Freundlich, and Sips isotherm) and kinetic diffusion models (Fickian and non-Fickian diffusion models). The degree of ATN release was further investigated using an artificial skin test to evaluate the drug release mechanism and the application as a TDDS. Moreover, functional thermo-sensitive ALP imprinted biomaterials were prepared with press needles and ALP release behavior was investigated.

2. Experimental

2.1. Materials

Allopurinol (ALP), poloxamer 407 (PX), polyvinyl alcohol (PVA) (Mw: 89,000– 98,000 and the degree of hydrolysis (DH): 99%), sodium benzoate (SB) (Bioxtra >99.5%), dimethyl sulfoxide (DMSO), glycerol (GL), and xylitol (XL) were purchased from Sigma-Aldrich Chemical Company, Inc. (St. Louis, MO, USA). Mungbean starch (MBS) was obtained from Chungwon food (Incheon, South Korea). Press needles were purchased from Dongbang medical (South Korea). All other chemicals and materials were commercially available without further purification. Distilled water (DW) was re-distilled after deionization and used in all experiments.

2.2. Preparation of functional thermo-sensitive ALP imprinted MBS/PVA biomaterials

Functional thermo-sensitive ALP imprinted MBS/PVA biomaterials were prepared using a casting method and UV curing process. First, PX as a thermo-sensitive polymer was dissolved in DW (80 mL). Subsequently, MBS, SB, and plasticizers (GL or XL) is mixed with DW using a mechanical stirrer (400 rpm). PVA solution was then prepared by dissolving PVA in hot DW (95 °C). PVA solution and mixed MBS/SB/plasticizers were left at 95 °C for 10 min. The mixture was blended to form a homogeneous gel-like solution with a mechanical stirrer (600 rpm) at room temperature for 60 min. Imprinting of ALP as the target drug was performed as follows. After dissolving 0.5 g ALP in DW (20 mL), the ALP solution was added dropwise for 15 min to have a uniform gel-like solution during the blending process of MBS/PVA/SB/plasticizers. Compositions of functional thermo-sensitive ALP imprinted biomaterials are described in Table 1. Bubbles were removed using an aspirator and the gel-like solution was poured on to a pre-warmed (60 °C) teflon mold (200 × 200 × 1 mm). Water was evaporated from the mold in a ventilated oven at 50 °C for 24 h. Prepared biomaterials were then cured for 10, 20, 30, 40, 50, and 60 min using a UV lamp (OSRAM ULTRA-VITALUX, 300 W) at an atmospheric pressure. After the UV curing process, biomaterials were conditioned at 25 °C for one week with a relative humidity (RH) of 55%. In case of functional thermo-sensitive ALP imprinted biomaterials containing press needles, after the casting process of gel-like solution in the teflon mold, biomaterials were prepared by adding press needles before drying these biomaterials.

2.3. Characterization

To confirm functional groups of prepared functional thermo-sensitive MBS/PVA biomaterials with/without the addition of ALP, Fourier transform infrared spectrophotometry (FT-IR) analysis was performed using FT-IR spectrophotometer (vertex-70, Bruker, Germany). Surfaces and cross-sections of prepared biomaterials were investigated using a field emission scanning microscope (FE-SEM) (S-4700, Hitachi, Tokyo, Japan) at an acceleration voltage of 5.0 kV. ^{1}H nuclear magnetic resonance (^{1}H NMR) spectra were recorded on a Varian Unity Inova 500 MHz spectrometer at the Korea Basic Science Institute (KBSI, Gwangju Center, Korea). Samples for NMR analysis were dissolved in DMSO-d_6.

2.4. Mechanical properties

Tensile strength (TS) and elongation properties (%E) of prepared biomaterials were evaluated using an Instron 6012 testing machine (Norwood, MA, USA). Five dumbbell shaped specimens (ASTM D-412) were obtained by cutting biomaterials. The thickness of each biomaterial was measured at six places along the test length using a mechanical scanner (Digital thickness gauge "Mitutoyo" Tokyo, Japan) at 16–20 random positions around the prepared biomaterial. The average thickness of specimens was 0.105 ± 0.005 mm. Gauge length and grip distance were 50.0–55.0 mm. The crosshead speed was 20 mm/min and the load cell capacity was 250 kg_f. All tests were conducted at 25 °C with RH of 58.0%.

Table 1
The composition of functional thermos-sensitive ALP imprinted MBS/PVA biomaterials.

Sample name	MBS (g)	PVA (g)	PX (wt%)	GL (wt%)	XL (wt%)	SB (wt%)	ALP (g)	DW (g)
MBSP	6.0	4.0	–	–	–	–	–	100
MBSPSB1	6.0	4.0	–	–	–	1.0	–	100
MBSPSB2	6.0	4.0	–	–	–	2.0	–	100
MBSPSB3	6.0	4.0	–	–	–	3.0	–	100
MBSPSB4	6.0	4.0	–	–	–	4.0	–	100
MBSPSB5	6.0	4.0	–	–	–	5.0	–	100
MBSPSB3PX2.5	6.0	4.0	2.5	–	–	3.0	–	100
MBSPSB3PX5	6.0	4.0	5.0	–	–	3.0	–	100
MBSPSB3PX7.5	6.0	4.0	7.5	–	–	3.0	–	100
MBSPSB3PX10	6.0	4.0	10.0	–	–	3.0	–	100
MBSPSB3PX5-ALP	6.0	4.0	5.0	–	–	3.0	0.5	100
MBSPSB3PX5GL-ALP	6.0	4.0	5.0	40	–	3.0	0.5	100
MBSPSB3PX5XL-ALP	6.0	4.0	5.0	–	40	3.0	0.5	100

2.5. Water resistance properties

Swelling behavior, solubility, and contact angle analysis of prepared biomaterials were measured to verify their water resistance properties.

Dried biomaterials were immersed in distilled water at 25.0 °C. Surface moisture of each biomaterial was then removed after 24 h to reach equilibrium and the weight of each biomaterial was measured. Swelling behavior of each biomaterial was calculated using the following Eq. (1) [21]:

$$\text{Swelling behavior} = \frac{W_e - W_0}{W_0} \quad (1)$$

where W_e was the weight of the swelling biomaterial at equilibrium, and W_0 was the initial dry weight of the biomaterial.

Swollen biomaterials were dried again at 50 °C for 24 h. Solubility value of each biomaterial was calculated using the following Eq. (2):

$$\text{Solubility} = \frac{W_0 - W_d}{W_d} \quad (2)$$

where W_0 was the initial dry weight of the biomaterial and W_d was the dry weight of the swollen biomaterial.

Contact angle analysis was carried out as described by Youn et al. [22]. Contact angle with a change of temperature was analyzed using water droplet at 25, 36.5, and 45.0 °C. Water droplet images of biomaterials were taken with a digital camera and analyzed with a video capture program (ImageJ with drop analysis plug-in, National Institutes of Health, USA) for contact angle measurement. The light source was an LED flashlight (Cateye HL-AU230, brightness 250 cd, battery life 30 h). The sample holder used was a Thorlab GN05 that could be tilted ±15° to both sides. Canon EOS 450D camera equipped with a macro lens was used. Light source, sample holder, and the camera were all fixed to an optical plate (Thorlab 60 × 45 breadboard, MB4560 M).

2.6. Recognition properties

To investigate recognition properties of functional thermo-sensitive ALP imprinted biomaterials, ALP extraction was performed using a Soxhlet extraction process. Briefly, ALP imprinted biomaterial (0.20 g) was put into a Soxhlet equipment. ALP was then removed using co-solvent mixtures of DW and DMSO (6:4) for 12 h. Biomaterials were then cleaned with DMSO and DW alternately until no ALP was detected by a UV–vis spectrophotometer (OPTIZEN 2120UV, Neogen, Co., Ltd., Korea). Biomaterials in which ALP were removed using Soxhlet extraction process were dried in a vacuum oven at 50 °C for 12 h. Binding isotherm was obtained by adding a fixed amount of 0.1 g of biomaterials into a 45 mL vial containing 30 mL of different initial concentrations (0.20–1.0 mmol/L) of ALP. Vials were agitated in a shaking incubator (DS-210SF, Daewon science, Inc., Korea) at 100 rpm for 24 h at 25 °C until equilibrium was reached. Aqueous samples were then taken from these solutions and ALP concentrations were examined using a UV–vis spectrophotometer. The binding isotherm for non-imprinted ALP biomaterials was also determined using the same procedure to confirm effects of ALP recognition. The adsorbed amount (Q) of ALP bound to imprinted biomaterials was calculated using the following Eq. (3):

$$Q(\mu\text{mol/g}) = \frac{(C_i - C_e)V}{W} \quad (3)$$

where C_i and C_e were ALP concentrations (mmol/L) measured initially and at equilibrium, respectively. V was the volume of the solution (L) and W was the mass (g) of the dry imprinted biomaterials used.

2.7. ALP release properties

To evaluate the release properties of ALP in functional thermo-sensitive ALP imprinted biomaterials, effects of drug release were examined at pH 4.0, 7.0, and 10.0 with different temperature (25.0, 36.5, and 45.0 °C). Functional thermo-sensitive ALP imprinted biomaterials (0.10 g) were immersed in flasks containing 100 mL standard buffer solutions at pH 4.0, 7.0, and 10.0 [20]. These flasks were then incubated at 25.0, 36.5, or 45.0 °C on a shaking incubator (80 rpm). At predetermined time intervals, 2 mL supernatant of the solution was taken and released ALP was measured using a UV–vis spectrophotometer at 257.0 nm. The possibility of a TDDS was also confirmed via release test using an artificial skin (Neoderm-ED, Tego Science, Inc. Korea). Prepared functional ALP imprinted biomaterials (1.5 × 1.5 cm) were put on artificial skin on the agar based gel at 36.5 °C with RH of 60.0%. After a certain period of time, agar-based gel was immersed in DW at 25.0 °C for 3 h. Then, the degree of release of ALP was measured using UV–vis spectrophotometer. The release behavior of ALP in functional thermo-sensitive ALP imprinted biomaterials with/without the addition of a press needle was also investigated.

2.8. Statistical analysis

Experimental results of this study were evaluated for statistical significance using Student's *t*-test through repeated experiments. Test results are expressed as mean ± standard deviation (SD).

3. Results and discussion

3.1. Characterization of functional thermo-sensitive ALP imprinted MBS/PVA biomaterials

Investigating the preparation condition of functional biomaterials for application of a TDDS is important. To obtain an optimal preparation condition of functional thermo-sensitive ALP imprinted MBS/PVA biomaterials, swelling behavior and solubility that could be used to confirm the degree of crosslinking were examined. Fig. 1a, b, and c show swelling behavior and solubility results of functional biomaterials under various preparation conditions such as UV curing time, thermo-sensitive polymer contents (PX), and crosslinking agent contents (SB). As shown in Fig. 1a, swelling behavior and solubility values decreased drastically with increasing UV curing time. Such results are attributed to crosslinking reactions between components of biomaterials during UV curing process. With increasing content of SB as a crosslinking agent, swelling behavior and solubility values decreased rapidly (Fig. 1b). However, increases of swelling behavior and solubility occurred when UV curing time and SB content were more than 30 min and 3 wt%, respectively. Such results might be due to the fact that molecules with short length or short chains of crosslinked biomaterials were dissolved or degraded in DW as reported in previous studies [21]. Fig. 1c shows swelling behavior and solubility of UV cured biomaterials added with 3 wt% SB and PX. Results indicated that with an increase of PX content, swelling behavior also increased whereas solubility S decreased. Layer separation and non-uniformity of biomaterials occurred when more than 5 wt% PX was added. Based on these results, we prepared ALP imprinted MBS/PVA biomaterials using UV curing time of about 30 min, 3 wt% SB, and 5 wt% PX. In addition, we conducted contact angle analysis for biomaterials prepared using the above condition to verify their water resistance properties at different temperatures. Fig. 1d shows results of contact angle analysis for prepared biomaterials with/without the addition of GL and XL as plasticizers. Results showed that the contact angle decreased with an increase of temperature for biomaterials with/without the addition of PX. Contact angles were 1.15 times, 1.47 times, and 1.72 times lower at temperatures of 25 °C, 36.5 °C, and 45.0 °C, respectively. These results mean that PX added biomaterials have a thermo-sensitive property. In addition, GL or XL added biomaterials showed a thermo-sensitive property, although their contact angles were relatively smaller than those of biomaterials without the addition of GL or XL because of the hydrophilic property of plasticizers.

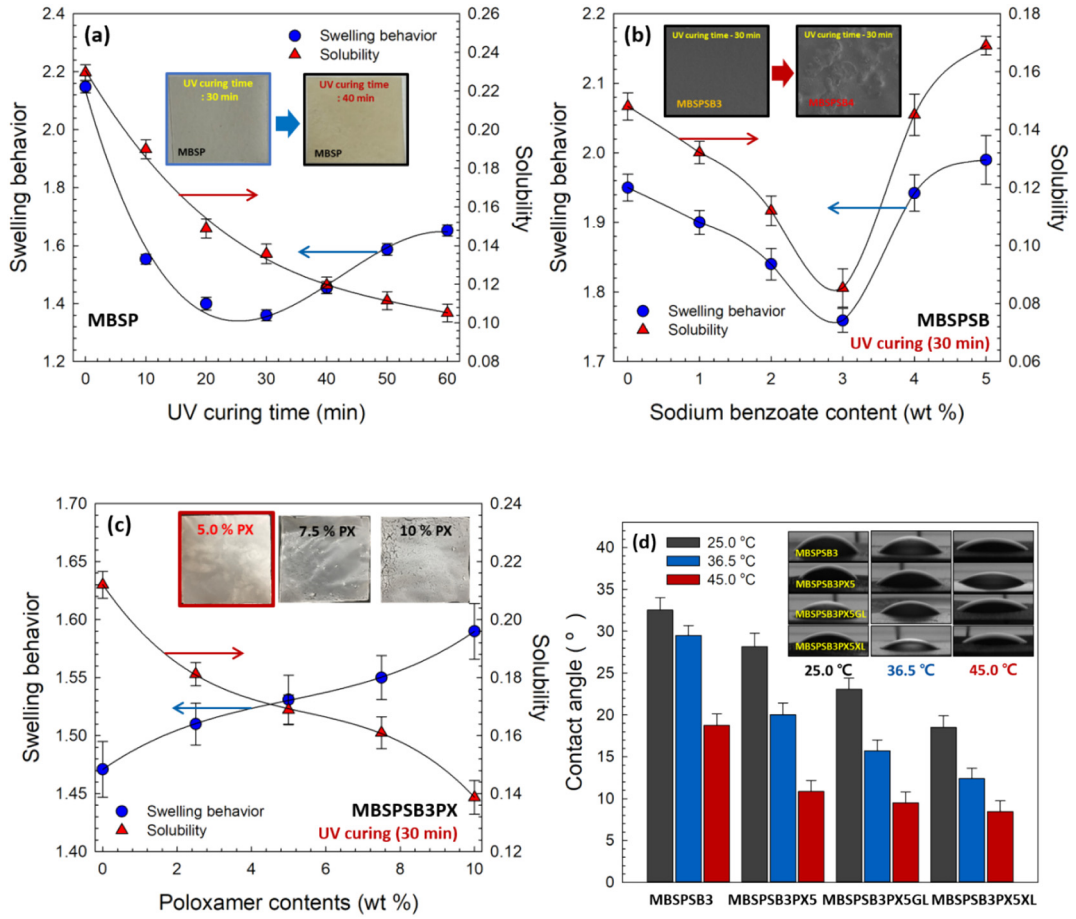

Fig. 1. Water resistance properties of MBS/PVA biomaterials. (a) Swelling behavior and solubility of MBS/PVA biomaterials with UV curing time. (b) Swelling behavior and solubility of MBS/PVA biomaterials with SB content. (c) Swelling behavior and solubility of MBS/PVA biomaterials with PX content. (d) Contact angle analysis at different temperatures of prepared MBS/PVA biomaterials.

To confirm the stability of ALP by UV irradiation and ALP imprint in functional biomaterials, UV irradiated ALP and prepared functional biomaterials were subjected to FT-IR and ^{1}H NMR analysis. Fig. 2a and b show FT-IR spectra and ^{1}H NMR before and after UV irradiation of ALP. Results indicated that the degradation of ALP did not occur under the synthesis condition of functional biomaterials. FT-IR spectra of characteristic peaks of ALP showed bands at 3178.9 and 1591.5 cm^{-1} due to N—H stretching vibrations, a band at 1700.3 cm^{-1} observed to C═O stretching, a band at 1482.6 cm^{-1} due to C═N stretching, a band at 1387.5 cm^{-1} due to C═C stretching, and a band 1237.6 cm^{-1} due to C—N asymmetrical stretching. The absorption binding at 2990.7 and 2885.3 cm^{-1} was ascribed to C—H stretching vibrations of proteins or the pyrimidine ring of ALP [23,24]. In addition, ^{1}H NMR spectrum of specific peaks of ALP appeared at 8.11 and 8.04 ppm for protons containing ALP chemical structure.

Fig. 2c shows results of FT-IR analysis for prepared biomaterials with/without the addition of ALP. In case of FT-IR spectra of non-imprinted biomaterials, absorption bands between 840.0 and 950.0 cm^{-1} can be assigned to -C-O-C- ring vibration in granular starch. In addition, peaks at 1116.5 and 1018.9 cm^{-1} corresponding to the anhydroglucose ring of starch were observed. Absorption bands appeared at 1335.2 and 1415.4 cm^{-1} were assigned to bending vibrations of -CH_2 in -O-CH_2. Broad absorption bands at 3419.2 and 3283.4 cm^{-1} as asymmetry and symmetry stretching were attributed to hydrogen bonded hydroxyl groups (-OH). Results of FT-IR analysis for functional ALP imprinted biomaterials with/without the addition of GL or XL verified that characteristic absorption peaks of ALP appeared at 1699.7 and 1591.8 cm^{-1}. However, other peaks could not be confirmed by overlapping with similar chemical bonds.

Fig. 3 shows SEM images of surface and cross-sections of prepared functional thermo-sensitive biomaterials with/without the addition of ALP and 40 wt% plasticizers (GL or XL). Results indicated showed no noticeable agglomeration, voids, porosity, or cracks in SEM images of surfaces and cross-sections of non-imprinted ALP biomaterials. Similar results were obtained for functional thermo-sensitive ALP imprinted biomaterials.

3.2. Mechanical properties

Investigating of mechanical properties of biomaterials is necessary before applying them in a TDDS because of various external environment factors. Table 2 shows results of tensile strength (TS) and elongation behavior (EB) for functional biomaterials with/without the addition of ALP and plasticizers (GL and XL). Results indicated that TS of functional biomaterials without the addition of plasticizers were higher than those of functional biomaterials containing plasticizers. In addition, EB values of GL or XL added functional biomaterials were higher than those of functional biomaterials without the addition of plasticizers. TS and EB values for functional ALP imprinted biomaterials were similar those of non-imprinted biomaterials. These results confirmed that functional biomaterials could be synthesized under various external conditions. In this study, the ALP extraction process was carried out to investigate recognition properties. Measuring changes in mechanical properties of biomaterials is important before applying them to various fields such as biosensor, functional adsorbent, functional coating materials, and so on. Results indicated that TS and EB were slightly decreased after the extraction process without showing significant changes in their mechanical properties.

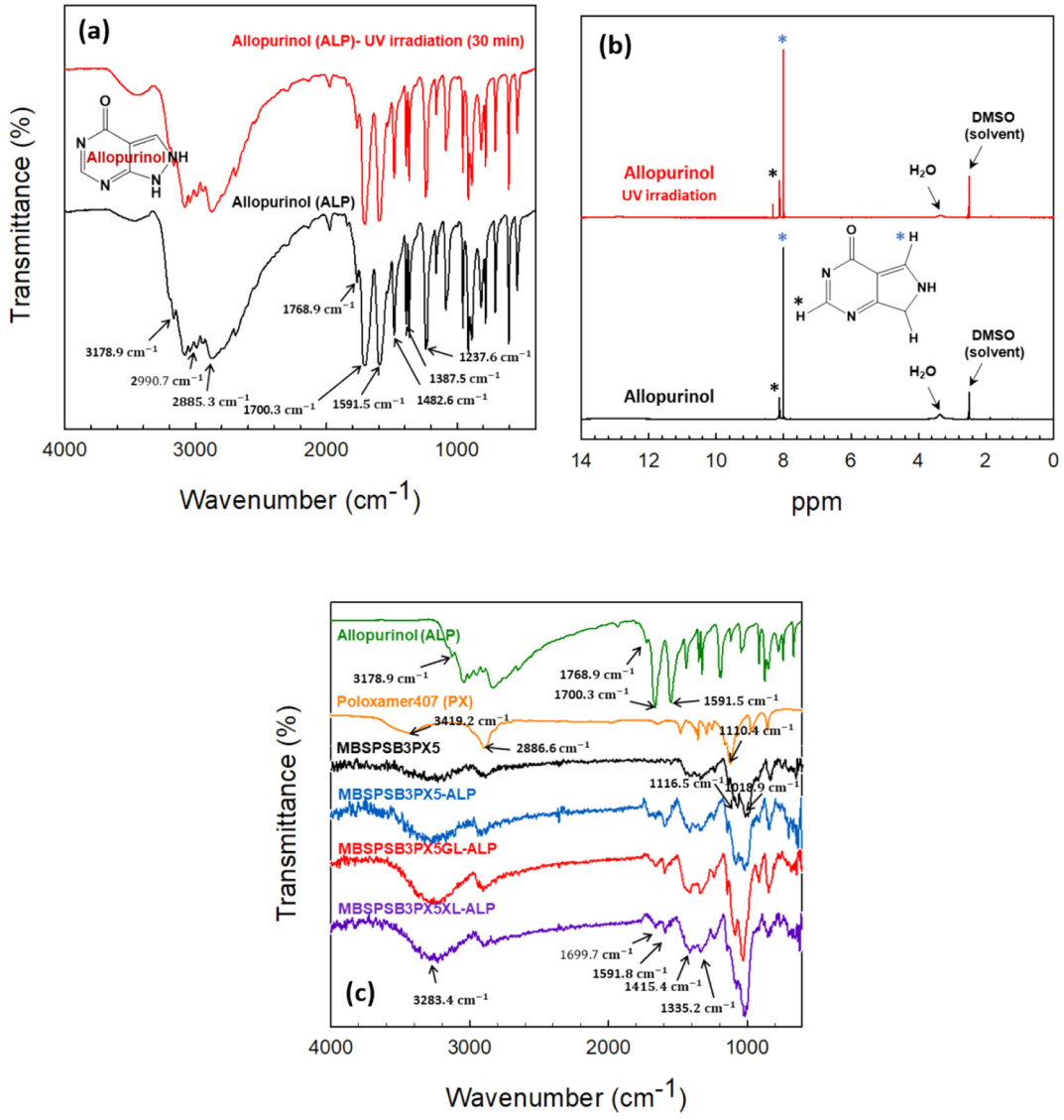

Fig. 2. FT-IR spectra and ^{1}H NMR of ALP with/without UV irradiation (a) and functional MBS/PVA biomaterials with/without the addition of ALP (b).

3.3. Recognition properties

Recognition properties should be considered for target drug imprinted biomaterials with practical applications such as quantitative analysis of optimal dose, target drug release control, and effective drug treatment [25]. Thus, recognition properties after ALP extraction were determined using adsorption isotherm and binding site energy distribution.

Results of the degree of ALP removal with the Soxhlet method using DW/DMSO mixture as co-solvents was shown in Fig. S1. The extraction efficiency of ALP was calculated as the degree of ALP extraction ratio (%) into functional ALP imprinted biomaterials (0.20 g). ALP extraction efficiency was above 98.5% for about 24 h at room temperature (Fig. S1). In addition, the rate of ALP extraction for functional biomaterials without the addition of plasticizers was faster than that of functional biomaterials added with GL or XL as plasticizers. This result suggests that functional groups (hydroxyl groups) having plasticizers and ALP are linked by hydrogen bonding.

Fig. 4 shows results of adsorption isotherm for ALP in functional ALP imprinted biomaterials. The adsorbed amount (Q) was gradually increased with an increase of ALP concentration. Results verified that Q values of ALP on functional ALP imprinted biomaterials were 3.8–4.9-fold higher than those of non-ALP imprinted biomaterials. Results also indicated that Q values of functional ALP imprinted biomaterials added with PX, GL, or XL were 1.2–1.8-fold higher than those of functional ALP imprinted biomaterials without the addition of PX, GL, or XL. These results can be explained by the fact that binding sites or cavities that can adsorb ALP are relatively well formed by hydroxyl groups as functional groups of PX, GL, and XL. Adsorption properties of prepared functional ALP imprinted biomaterials were also analyzed using Langmuir, Freundlich, and Sips isotherm equation. Model isotherm equations used in this study are summarized in Table 3. Parameters' values of adsorption isotherms were obtained with the Nelder-Mead method [26]. The error between experimental and calculated values was compared by regression analysis values.

Fig. 4 and Table S1 show adsorption isotherm (symbols) on functional ALP imprinted biomaterials and their corresponding fitting curves by Langmuir, Freundlich, and Sips isotherm equation. Results indicated that fitting curves for isotherm data of non-imprinted biomaterials well matched with Langmuir and Sips isotherms. However, results of isotherm data of functional ALP imprinted biomaterials indicated that the fitting ability of Sips and Freundlich isotherms was superior to that of the Langmuir isotherm. The Langmuir isotherm assumes monolayer adsorption onto homogeneous surface of an adsorbent. If the adsorption

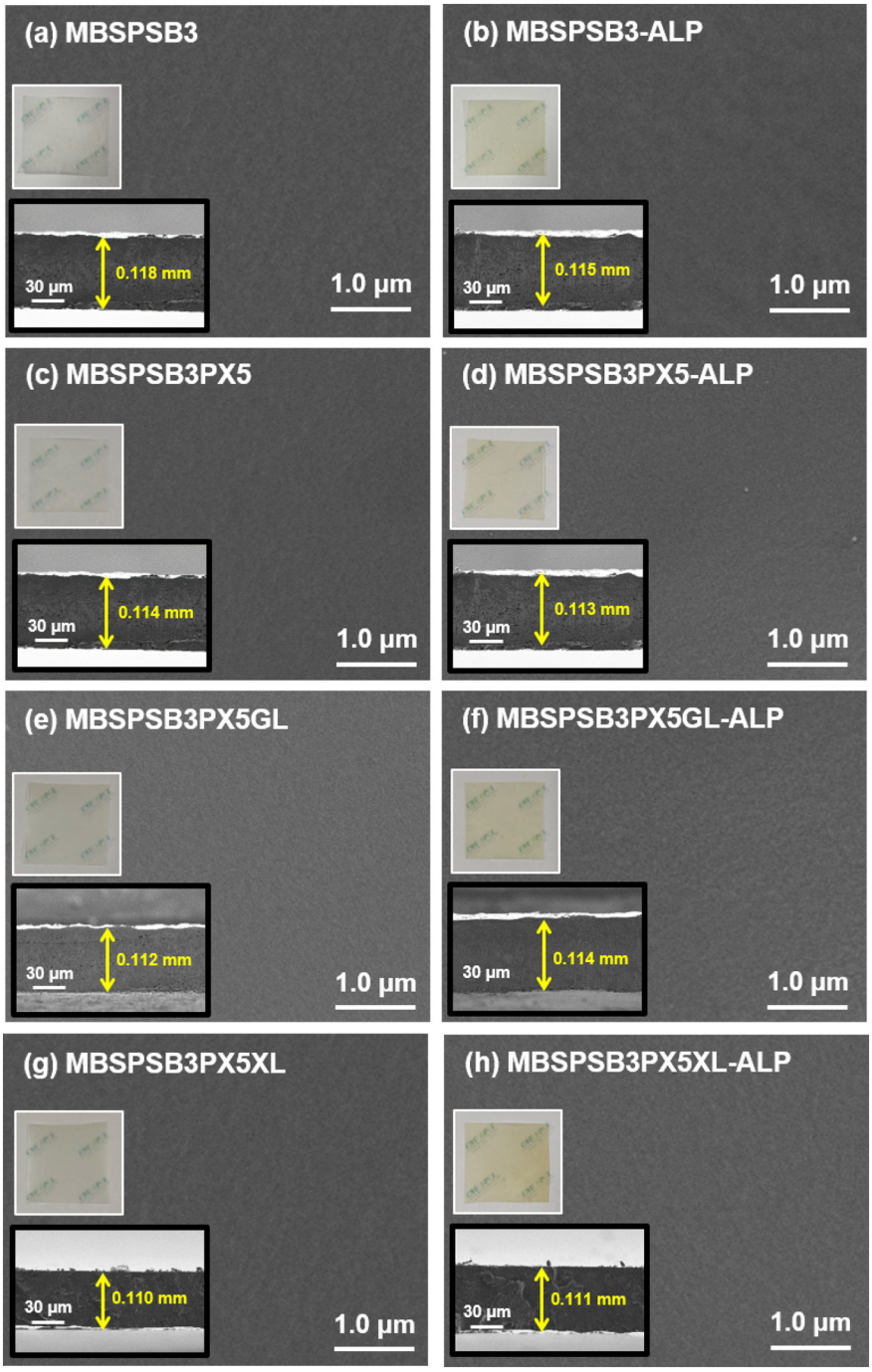

Fig. 3. SEM images of surfaces and cross-sections of functional biomaterials. (a) non-imprinted biomaterial. (b) ALP imprinted biomaterial without the addition of plasticizers. (c) Functional non-imprinted biomaterial without the addition of plasticizers. (d) Functional ALP imprinted biomaterial without the addition of plasticizers. (e) Functional non-imprinted GL-added biomaterial. (f) Functional ALP imprinted GL-added biomaterial. (g) Functional non-imprinted XL-added biomaterial. (h) Functional ALP imprinted XL-added biomaterial.

site is filled with an adsorbate, there is no adsorption in the adsorption site. In addition, a homogeneous surface of an adsorbent is energetically uniform without interaction between adsorbates [27]. As shown in Table S1, n_s values of Sips isotherm for non-imprinted biomaterials (MBSPSB3 and MBSPSB3PX5) were 1.049 and 1.062, respectively. Such n_s value for Sips isotherm means that if it is close to 1.0, the surface of non-imprinted biomaterials can be considered as energetically uniform. Therefore, it could be known that a unimolecular adsorption on a homogeneous surface was achieved when the surface of non-imprinted biomaterials was covered with ALP as the target molecule. In case of functional ALP imprinted biomaterials, the parameter n_s value of Sips isotherm and the parameter n_F value of the Freundlich isotherm related to the heterogeneity of adsorption energy deviated from 1.0, indicating that surfaces of functional ALP imprinted biomaterials were more energetically nonuniform than that of non-imprinted biomaterials. In addition, results suggest that there is a binding site for ALP as the target molecule. To verify the binding site for prepared functional biomaterials, binding site energy distribution was investigated using the relationship of adsorption energy or the affinity between ALP and functional ALP imprinted biomaterials [21,28]. It was

Table 2
Mechanical properties of functional thermos-sensitive ALP imprinted MBS/PVA biomaterials.

Sample name	Tensile strength (MPa)		Elongation at break (%)	
	Before extraction	After extraction	Before extraction	After extraction
MBSP	69.4 ± 1.61	–	14.2 ± 1.21	–
MBSPSB3	71.8 ± 1.47	–	12.8 ± 1.36	–
MBSPSB3PX5	74.9 ± 1.37	–	22.7 ± 1.28	–
MBSPSB3PX5-ALP	76.2 ± 1.68	71.6 ± 1.41	20.8 ± 1.41	17.3 ± 1.52
MBSPSB3PX5GL	16.9 ± 1.31	–	97.6 ± 1.53	–
MBSPSB3PX5GL-ALP	19.1 ± 1.40	17.4 ± 1.57	94.7 ± 1.48	91.7 ± 1.47
MBSPSB3PX5XL	24.6 ± 1.50	–	88.1 ± 1.38	–
MBSPSB3PX5XL-ALP	27.8 ± 1.53	23.4 ± 1.35	85.4 ± 1.36	79.7 ± 1.43

Table 3
List of single component adsorption isotherm equations used in this study.*

Isotherm	Mathematical form	Parameter
Langmuir	$Q = \frac{Q_m b_L C}{1+b_L C}$	Q_m [μmol/g] b_L [L/mmol]
Freundlich	$Q = K_F P^{1/n_F}$	K_F [(μmol/g)·(L/mmol)$^{1/nF}$] n_F [-]
Sips	$Q = \frac{Q_m b_S C^{1/n_S}}{1+b_S C^{1/n_S}}$	Q_m [μmol/g] b_S [L/mmol] n_S [-]

* where Q_m is the amount of target drug (ATN) adsorbed (μmol/g) on the ATN imprinted biomaterial patches at equilibrium, and b_L, K_F, b_S, n_F, n_S are the isotherm parameters of Langmuir, Freundlich, and Sips equations.

calculated based on the binding site energy distribution function as shown in Eq. (4):

$$\theta_t(c) = \int_0^{x_{max}} \theta_l(c,x)\, f(x) dx \tag{4}$$

where θ_t (c) was binding isotherm data, θ_l (c, x) was a local binding isotherm with binding energy, $f(x)$ was the function of binding site energy distribution, and c and x were equilibrium concentration and adsorption energy, respectively. Herein, binding site energy distribution was calculated using the Langmuir isotherm and the generalized regularization method.

Fig. 5 shows binding site energy distribution of non-imprinted functional biomaterials and functional ALP imprinted biomaterials with/without the addition of PX, GL, and PX. Results showed clear differences in binding site energy distribution for functional biomaterials with/without ALP imprinting. In addition, the single binding site energy distribution curve was obtained for non-imprinted functional biomaterials, whereas two binding site energy distribution curves for low and high binding energy ranges were obtained for functional ALP imprinted biomaterials. These results confirmed that there was the specific binding site that could adsorb ALP as the target molecule. Low and high binding energy values for functional ALP imprinted biomaterials were in the following order: MBSPSB3PX5XL-ALP

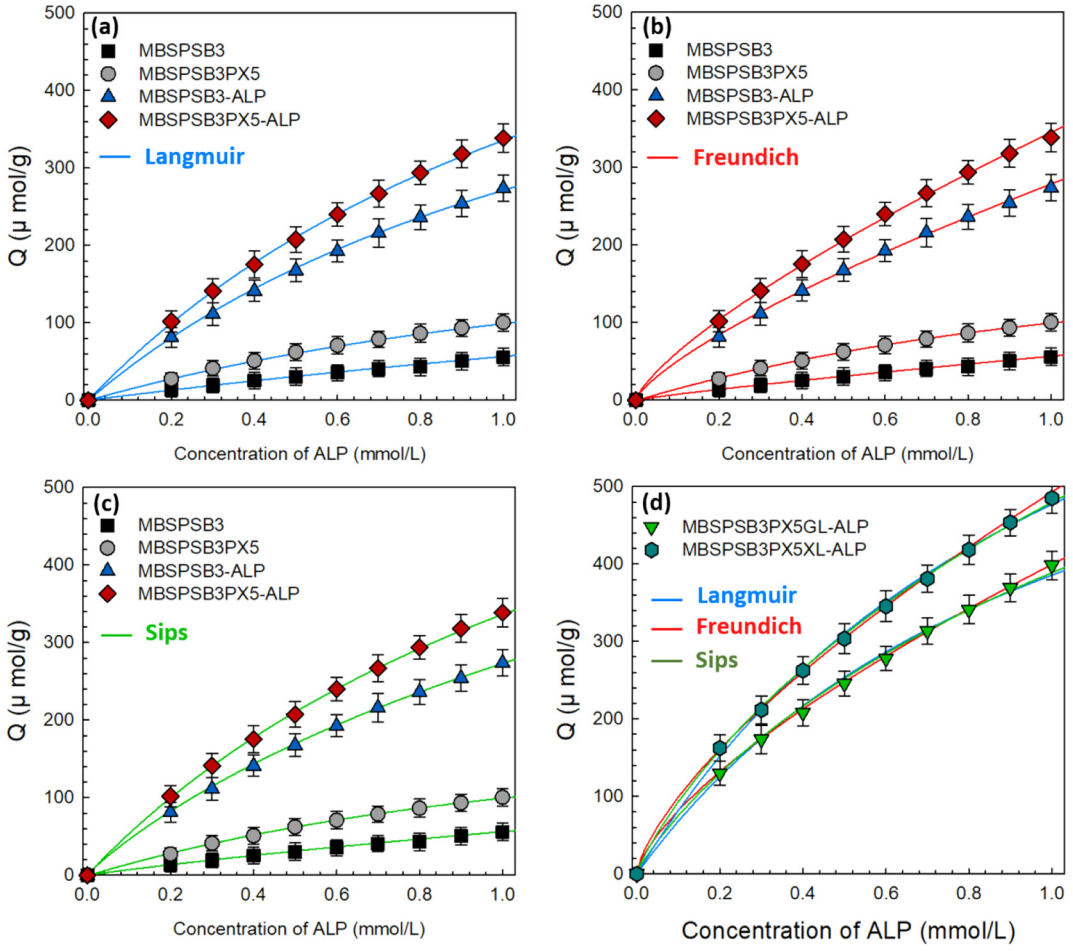

Fig. 4. Adsorption isotherms (symbols) on functional ALP imprinted biomaterials and their corresponding fitting to Langmuir isotherm (a), Freundlich isotherm (b), and Sips isotherm (c) (lines). (d) Adsorption isotherms (symbols) on functional ALP imprinted biomaterials added with GL and XL and their corresponding fitting to Langmuir, Freundlich, and Sips isotherm (lines).

(0.0037 and 21.711 L/mol) > MBSPSB3PX5GL-ALP (0.0034 and 15.344 L/mol) > MBSPSB3PX5-ALP (0.0026 and 2.705 L/mol) > MBSPSB3-ALP (0.0024 and 0.675 L/mol). These results were similar to the order of Q values mentioned earlier. Thus, it was verified that the binding energy of functional ALP imprinted biomaterials added XL was the strongest and that the number of binding sites for ALP was higher than that of the orders.

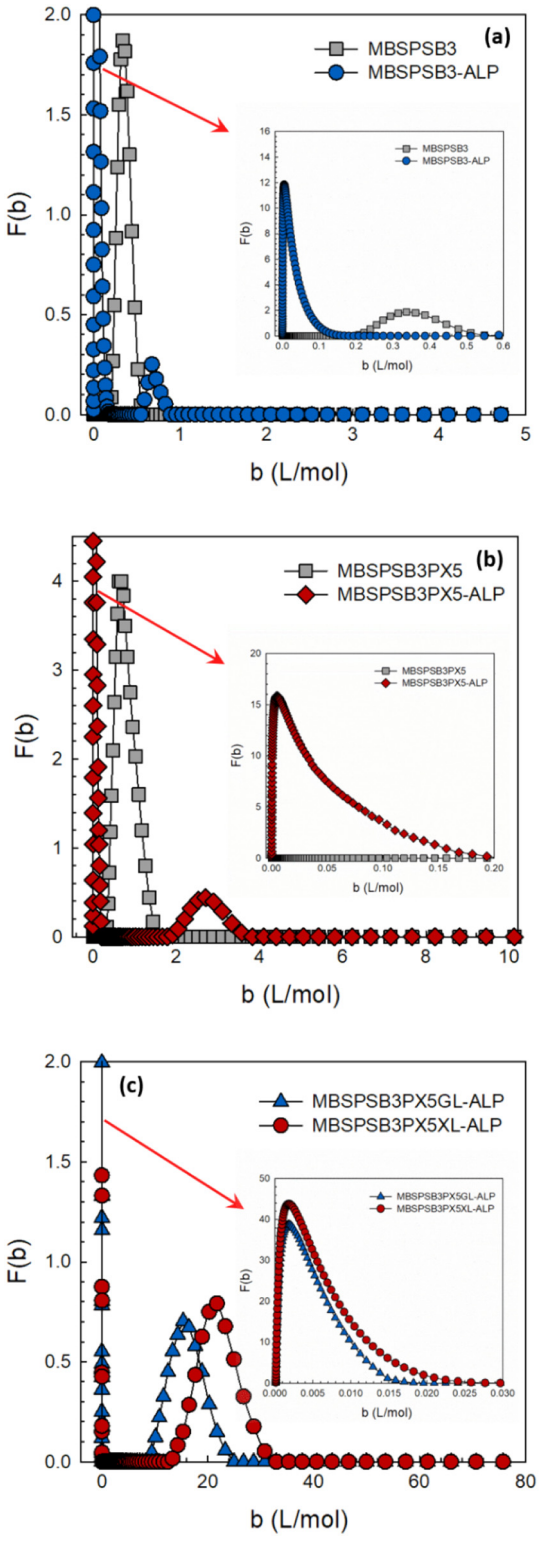

Fig. 5. Binding site energy distribution curves of ALP on functional ALP imprinted biomaterials. (a) Biomaterial with/without the addition of ALP. (b) Functional biomaterial with/without the addition of ALP. (c) Functional ALP imprinted biomaterial added with GL and XL.

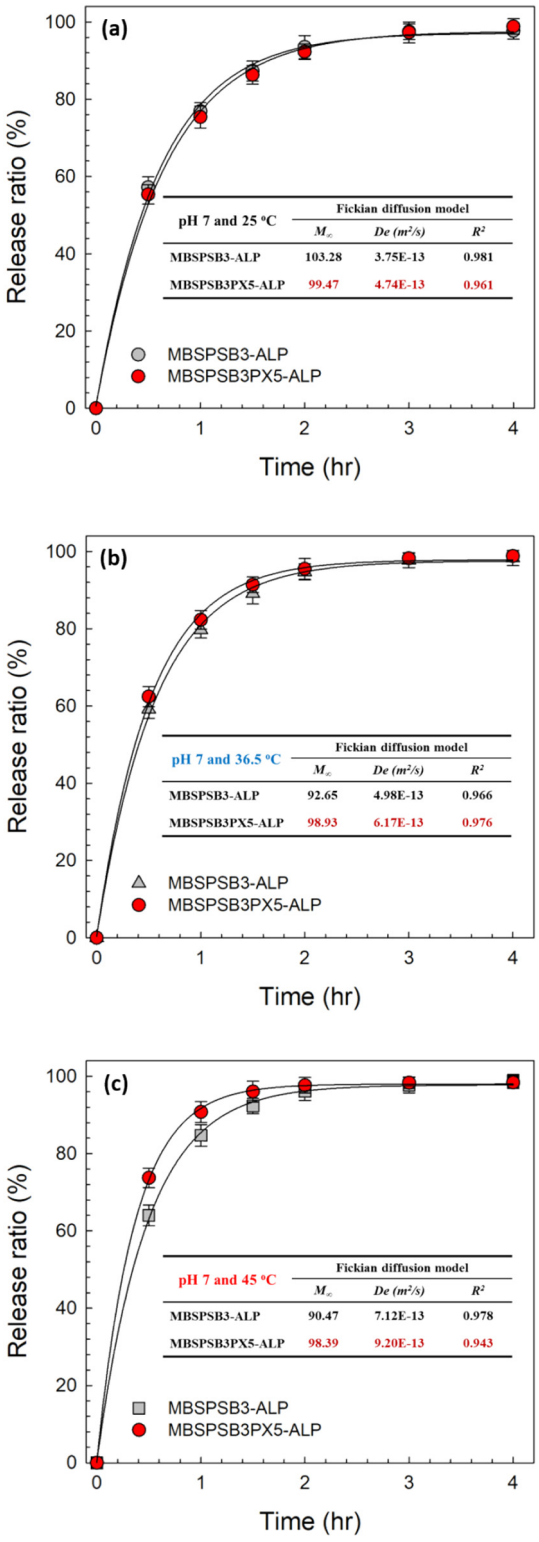

Fig. 6. ALP release ratio (%) from ALP imprinted biomaterials with/without the addition of PX at different temperatures. (a) ALP release ratio (%) from ALP imprinted biomaterials with/without the addition of PX at pH 7 and 25 °C. (b) ALP release ratio (%) from ALP imprinted biomaterials with/without the addition of PX at pH 7 and 36.5 °C. (c) ALP release ratio (%) from ALP imprinted biomaterials with/without the addition of PX at pH 7 and 45 °C.

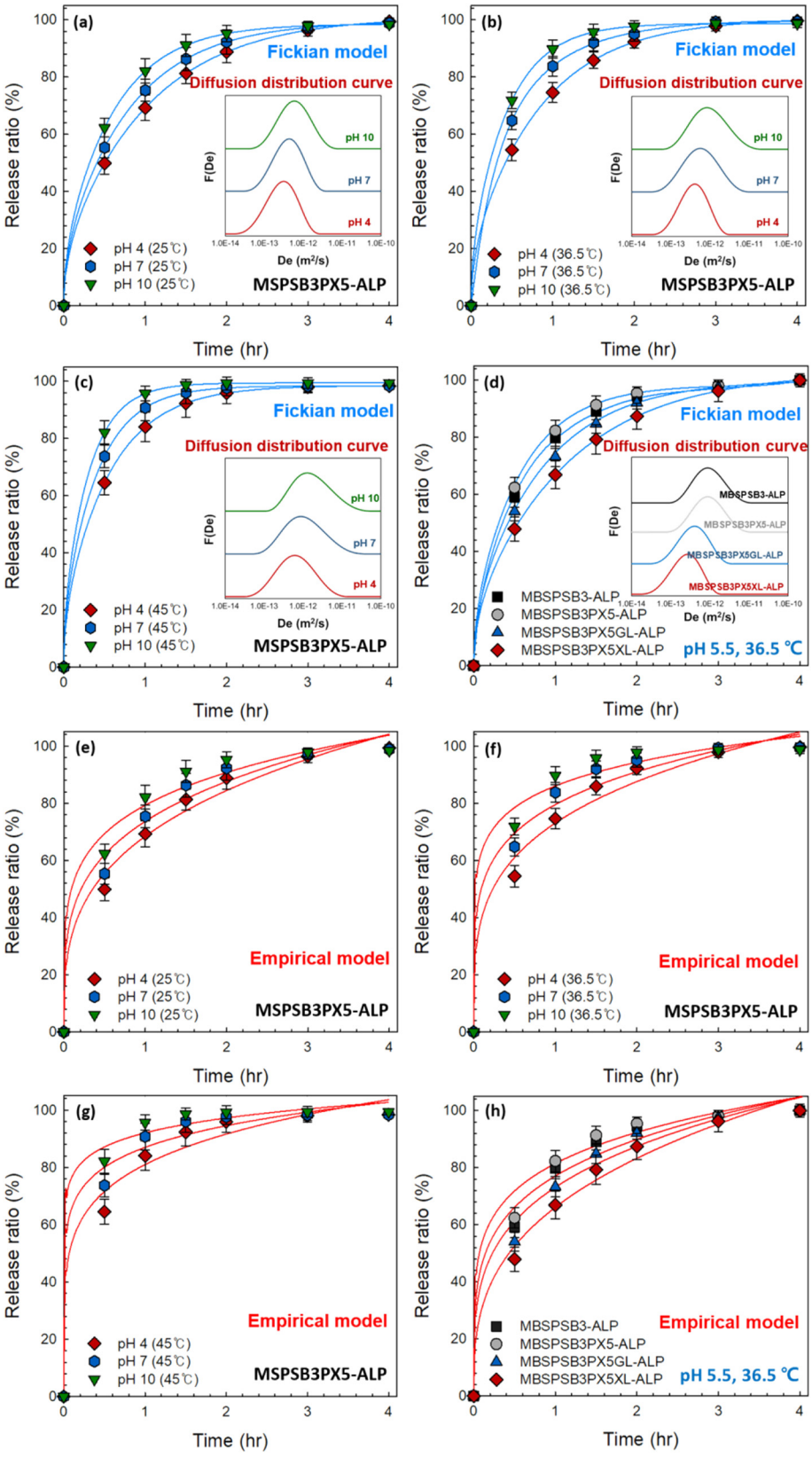

Fig. 7. Experimental and Fickian model fits of ALP release ratio (%) from functional ALP imprinted biomaterials at different pHs and temperatures and their Fickian effective diffusion distribution curves (a-d) and experimental and empirical model fits of ALP release ratio (%) from ALP imprinted biomaterials at different pHs and temperatures (e-h).

3.4. ALP release properties

ALP release profiles at different pH values and temperatures for functional ALP imprinted biomaterials are shown in Figs. 6 and 7. In this study, the drug release mechanism was further evaluated using Fickian diffusion and empirical models for systematic analysis of ALP release behavior. Fickian diffusion model was obtained using Fick's diffusion as shown in the following Eq. (5) [29–31]:

$$\frac{\partial C}{\partial t} = D\frac{\partial^2 C}{\partial x^2} \tag{5}$$

where C was the concentration at time t and D was the constant diffusion coefficient.

The solution of Eq. (5) rearranged by the form of a trigonometric series was known as the Fickian diffusion model Eq. (6).

$$\frac{M_t}{M_\infty} = 1 - \sum_{n=0}^{\infty} \frac{8}{(2n+1)^2 \cdot \pi^2} \; exp\left[-\frac{D_e \cdot (2n+1)^2 \cdot \pi^2}{l^2} \cdot t\right] \tag{6}$$

where M_t was the drug release amount at time t, M_∞ was the drug release amount at infinite time, and l, t, and D_e were half-thickness of slab, diffusion time, and diffusion coefficient, respectively.

In addition, the diffusion distribution function Eq. (7) for drug release was obtained using Eq. (6):

$$M_t = M_\infty \int_{D_{e-min}}^{D_{e-max}} \left\{1 - \sum_{n=0}^{\infty} \frac{8}{(2n+1)^2 \cdot \pi^2} \; exp\left[-\frac{D_e \cdot (2n+1)^2 \cdot \pi^2}{l^2} \cdot t\right]\right\} \cdot f(D_e)\, dD_e \tag{7}$$

Additionally, the non-Fickian model was represented by the following empirical relation (8) [32,33]:

$$\frac{M_t}{M_\infty} = kt^n \tag{8}$$

where, k was the drug release constant and n was the diffusional exponent in terms of the drug release mechanism. Values of k and n were found by fitting data. The Fickian diffusion mechanism was characterized by $n = 0.5$, while n value between 0.5 and 1.0 indicated a non-Fickian mechanism.

Fig. 6 shows results of ALP release (%) of functional ALP imprinted biomaterials with/without PX as a thermo-sensitive polymer at different temperatures and pH 7. Results verified that the degree of ALP release increased with an increase of temperature. In addition, when compared to the ALP release rate calculated by Fickian diffusion model for functional ALP imprinted biomaterials with/without PX, the release rate at 25 °C was almost similar, whereas the release rate for PX added ALP imprinted biomaterials was 1.10 times (at 36.5 °C) or 1.30 times (at 45 °C) faster than that at 25 °C. These results indicate that functional ALP imprinted biomaterials have thermo-sensitive properties due to the addition of PX as a thermo-sensitive polymer. This suggests that if PX added biomaterial is applied to the fever area when there is a fever caused by pain, the drug release will become easier and the therapeutic effect can be high.

Fig. 7, Tables S2, and S3 show the results of ALP release (%) and Fickian diffusion and empirical model parameters from functional ALP imprinted biomaterials with/without the addition of plasticizers at different pH values and temperatures. In addition, we investigated the degree of ALP release using the diffusion distribution curve calculated by generalized regularization for ALP release. In case of functional ALP imprinted biomaterials without the addition of plasticizers, the ALP release (%) was more than 99.0% within 3 h. Results indicated that the degree of ALP release at pH 10 and 45 °C was higher than that at pH 4 and 25 °C. This result could also be verified by the diffusion distribution curve. The reason is because ALP dissolves well at high pH levels. ALP release for prepared functional ALP imprinted biomaterials under human skin conditions (pH 5.5 and 36.5 °C) is shown in Fig. 7d and h. Results revealed that there were significant differences in ALP release depending on the type of plasticizers added to functional ALP imprinted biomaterials with the following order: MBSPSB3PX5-ALP > MBSPSB3-ALP > MBSPSB3PX5GL-ALP > MBSPSB3PX5XL-ALP. The high release rate of ALP for non-added plasticizers functional ALP imprinted biomaterials containing PX is due to thermo-sensitive effects by the addition of PX as a thermo-sensitive polymer. In addition, the degree of ALP release in XL added functional ALP imprinted biomaterial was relatively lower than that of XL added functional ALP imprinted biomaterials. This might be related to the effect of large amounts functional groups (hydroxyl groups). ALP release rates calculated by Fickian diffusion model showed the following order: 8.90E-13 m^2/s (MBSPSB3PX5-ATN) > 8.05E-13 m^2/s (MBSPSB3-ATN) > 4.91E-13 m^2/s (MBSPSB3PX5GL-ATN) > 2.19E-13 m^2/s (MBSPSB3PX5XL-ATN). As shown in Fig. 7 (line), ALP release determined using Fickian diffusion model was more satisfactory than that using the empirical model.

3.5. ALP release using artificial skin

Physical properties and release behavior for prepared functional ALP imprinted biomaterials were described in the previous results section. To verify their applicability as a TDDS, the ALP release experiment was performed using artificial skin. For treating acute gout, we further

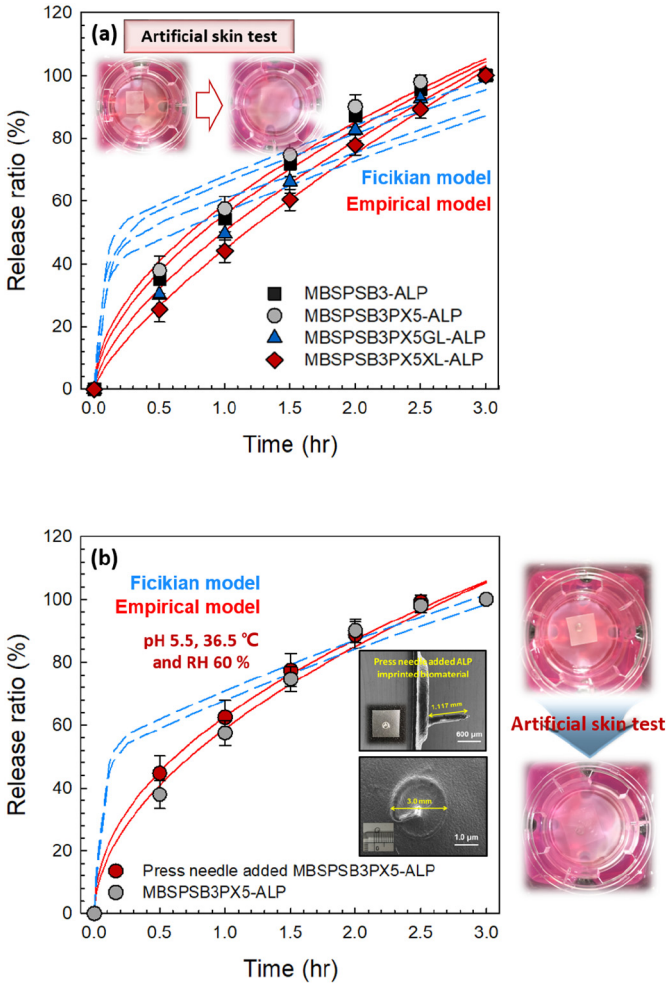

Fig. 8. ALP release ratio (%) from functional ALP imprinted biomaterials using artificial skin (a) and ALP release ratio (%) from functional ALP imprinted biomaterials added with press needles using artificial skin. The symbols represent experimental results and the long dash line (Fickian) and solid line (empirical) depict model prediction.

Table 4
Fickian diffusion and empirical model parameters of ALP release from different ALP imprinted MBS/PVA biomaterials using artificial skin at pH 5.5, 36.5 °C, and RH 60%.

Samples	Fickian diffusion model			Empirical model			
	M_∞	D_e	R^2	M_∞	k	n	R^2
MBSPSB3-ALP	1206.5 ± 30.12	1.04E-15	0.613	50.23 ± 1.21	1.109	0.572	0.983
MBSPSB3PX5-ALP	1245.3 ± 25.67	1.35E-15	0.593	52.47 ± 1.43	1.122	0.530	0.988
MBSPSB3PX5GL-ALP	1144.8 ± 20.34	9.35E-16	0.429	46.54 ± 1.07	1.083	0.651	0.991
MBSPSB3PX5XL-ALP	1031.4 ± 18.91	8.29E-16	0.451	42.53 ± 1.12	1.050	0.750	0.981
Press needle added MBSPSB3PX5-ALP	1274.3 ± 29.64	1.50E-15	0.434	55.08 ± 1.51	1.1398	0.511	0.985

prepared functional ALP imprinted biomaterials with the addition of press needles commonly used in oriental medicine and investigated their ALP release behaviors.

The ALP release profiles from functional ALP imprinted biomaterials using artificial skin at pH 5.5, temperature of 36.5 °C, and RH of 60% are shown in Fig. 8a. The amount of ALP release from functional ALP imprinted biomaterials was increased in a relatively steady-state rate with an increase of release time. The cumulative release was almost 98.1–99.1% for 3 h. Degrees of ALP release from functional ALP imprinted biomaterials depending on the type of plasticizers were found to have the following order: MBSPSB3PX5-ATN > MBSPSB3-ALP > MBSPSB3PX5GL-ALP > MBSPSB3PX5XL-ALP. As shown in Fig. 8a (line), the ALP release calculated using the empirical model was more satisfactory than that with the Fickian diffusion model. Based on results shown in Table 4, the diffusional exponent (n) of functional ALP imprinted biomaterials calculated by the empirical model was greater than 0.5, clearly indicating that ALP release behavior in artificial skin test followed the non-Fickian mechanism.

Fig. 8b represents results of ALP release (%) and ALP release behavior for functional ALP imprinted biomaterials with/without the addition of press needles. It was revealed that ALP release from press needles added functional ALP imprinted biomaterial was 1.15 times higher than that from functional ALP imprinted biomaterial without the addition of press needles. ALP release behavior further followed a non-Fickian mechanism because n value determined using the empirical model was greater than 0.5 (see Table 4). These results suggest that the use of press needles on biomaterials for a TDDS could be helpful for treating acute patients and designing a drug release control.

4. Conclusions

Functional allopurinol (ALP) imprinted biomaterials using MBS, PVA, PX, and plasticizers (GL and XL) were successfully synthesized using a UV curing process and casting methods. To determine optimum conditions for the preparation of functional ALP imprinted biomaterials, swelling behavior, solubility, and contact angle analysis were investigated with different UV curing time, crosslinking agent (SB) contents, and thermo-sensitive polymer (PX) contents. Optimum conditions were found to be as follows: UV curing time, 30 min; SB content, 3.0 wt%; and PX content, 5.0 wt%. ALP recognition properties for prepared functional ALP imprinted biomaterials were investigated using adsorption isotherm and binding site energy distribution function. Results indicated that adsorbed amounts (Q) of ALP on functional ALP imprinted biomaterials were 3.8–4.9-fold higher than those of non-ALP imprinted biomaterials. The adsorption characteristics of ALP on ALP imprinted biomaterials analyzed using Langmuir, Freundlich, and Sips isotherm equations were better explained by Freundlich and Sips equations than by the Langmuir equation. In addition, results of binding site energy distribution function confirmed that functional ALP imprinted biomaterials had two binding site energies related to ALP as the target drug. To verify the applicability to a TDDS for functional ALP imprinted biomaterials, ALP release properties were investigated at different pH values and temperatures. Results indicated that the degree of ALP release at a high pH and a high temperature was higher than that at a low pH and a low temperature. Especially, it could be confirmed that functional ALP imprinted biomaterials had thermo-sensitive properties due to the addition of PX as a thermo-sensitive polymer. Results of the analysis of ALP release behavior calculated by Fickian diffusion and empirical models indicated that ALP release could be satisfactorily explained by Fickian diffusion model and Fickian diffusion distribution function. In addition, results of ALP release using artificial skin indicated that the ALP release was increased at a relatively steady-state rate for 3 h. Results revealed that ALP release of press needles added functional ALP imprinted biomaterial was 1.15 times higher than that of functional ALP imprinted biomaterial without the addition of press needles. These results were explained by the empirical models, suggesting that the ALP release behavior followed the non-Fickian diffusion mechanism.

Acknowledgments

This research was supported by Basic Science Research Program through the National Research Foundation of Korea (NRF) funded by the Ministry of Education (Grant no. NRF- 2019R1I1A3A01061508).

Appendix A. Supplementary data

Supplementary data to this article can be found online at https://doi.org/10.1016/j.ijbiomac.2021.02.004.

References

[1] Y. Zhu, B. Pandya, H.K. Choi, Prevalence of gout and hyperuricemia in the US general population: the National Health and Nutrition Examination Survey 2007–2008, Arthritis Rheumatol. 63 (2011) 3136–3141.
[2] T. Neogi, Gout, N. Engl. J. Med. 364 (2011) 443–452.
[3] H.K. Choi, G. Curhan, Independent impact of gout on mortality and risk for coronary heart disease, Circulation. 116 (2007) 894–900.
[4] E. Krishan, J.F. Baker, D.E. Furst, H.R. Schumacher, Gout and the risk of acute myocardial infarction, Arthritis Rheumatol. 54 (2006) 2688–2696.
[5] H.K. Choi, M.A.D. Vera, E. Krishan, Gout and the risk of type 2 diabetes among men with a high cardiovascular risk profile, Rheumatology. 47 (2008) 1567–1570.
[6] A.B. Vargas-Santos, C.E. Peloquin, Y. Zhang, Association of chronic kidney disease with allopurinol use in gout treatment, JAMA Intern. Med. 178 (2018) 1526–1533.
[7] L.K. Stamp, R.O. Day, J. Yun, Allopurinol hypersensitivity: investigating the cause and minimizing the risk, Nat. Rev. Rheumatol. 12 (2016) 235–242.
[8] A.Z. Wilczewska, K. Niemirowicz, K.H. Markiewicz, H. Car, Nanoparticles as drug delivery systems, Pharmacol. Rep. 64 (2012) 1020–1037.
[9] P. Desai, R.R. Patlolla, M. Singh, Interaction of nanoparticles and cell-penetrating peptides with skin for transdermal drug delivery, Mol. Membr. Biol. 27 (2010) 247–259.
[10] Y. Zhang, H.F. Chan, K.W. Leong, Advanced materials and processing for drug delivery: the past and the future, Adv. Drug Deliv. Rev. 65 (2013) 104–120.
[11] A.W. Oosten, J.A. Abrantes, S. Jonsson, P. de Bruijn, E.J. Kuip, A. Falcao, C.C.D. van der Rijt, R.H. Mathijssen, Treatment with subcutaneous and transdermal fentanyl: results from a population pharmacokinetic study in cancer patients, Eur. J. Clin. Pharmacol. 72 (2016) 459–467.
[12] H. Lee, C. Song, S. Baik, D. Kim, T. Hyeon, D.H. Kim, Device-assisted transdermal drug delivery, Adv. Drug Deliv. Rev. 127 (2018) 35–45.
[13] G. Hamidreza, P. Kopecková, J. Kopecek, In vitro degradation of pH-sensitive hydrogels containing aromatic azo bonds, Biomaterials 18 (1997) 861–872.
[14] Y. Qui, K. Park, Environment-sensitive hydrogels for drug delivery, Adv. Drug Deliv. Rev. 53 (2001) 321–339.
[15] H.G. Schild, Poly(N-isopropylacrylamide): experiment, theory and application, Prog. Polym. Sci. 17 (1992) 163–249.
[16] S. Nadaf, A. Jadhav, S. Killedar, Mung bean (Vigna radiata) porous starch for solubility and dissolution enhancement of poorly soluble drug by solid dispersion, Int. J. Biol. Macromol. 167 (2021) 345–357.

[17] C.P. Palanisamy, B. Cui, H. Zhang, S. Jayaraman, G.K. Muthukaliannan, A comprehensive review on corn starch-based nanomaterials: properties, simulations, and applications, Polym. 12 (2020) 2161–2187.
[18] A.M. dos Santos, A.B. Meneguin, D.T. Akhter, N. Fletcher, Z.H. Houston, C. Bell, K.J. Thurecht, M.P.D. Gremião, Understanding the role of colon-specific microparticles based on retrograded starch/pectin in the delivery of chitosan nanoparticles along the gastrointestinal tract, Eur. J. Pharm. Biopharm. 156 (2021) 371–378.
[19] H.S. Kim, K.J. Kim, M.W. Lee, S.Y. Lee, Y.H. Yun, W.G. Shim, S.D. Yoon, Preparation and release properties of arbutin imprinted inulin/polyvinyl alcohol biomaterials, Int. J. Biol. Macromol. 161 (2020) 763–770.
[20] H.Y. Tak, Y.H. Yun, C.M. Lee, S.D. Yoon, Sulindac imprinted mungbean starch/PVA biomaterial films as a transdermal drug delivery patch, Carbohydr. Polym. 208 (2019) 261–268.
[21] H.S. Kim, Y.H. Yun, W.G. Shim, S.D. Yoon, Preparation of atenolol imprinted polysaccharide based biomaterials for a transdermal drug delivery system, J. Drug Deliv. Sci. Technol. 59 (2020) 101893.
[22] H.G. Youn, J.Y. Je, C.M. Lee, S.D. Yoon, Inulin/PVA biomaterials using thiamine as an alternative plasticizer, Carbohydr. Polym. 220 (2019) 86–94.
[23] A. Gerega, L. Lapinski, I. Reva, H. Rostkowska, M.J. Nowak, UV-induced generation of rare tautomers of allopurinol and 9-methylhypoxanthine-a matrix isolation FTIR study, Biophys. Chem. 122 (2006) 123–135.
[24] L. Deng, Y. Lia, F. Feng, D. Wu, H. Zhang, Encapsulation of allopurinol by glucose cross-linked gelatin/zein nanofibers: characterization and release behavior, Food Hydrocoll. 94 (2019) 574–584.
[25] L. Li, X. Ying, J. Liu, X. Li, W. Zhang, Molecularly imprinted polyurethane grafted calcium alginate hydrogel with specific recognition for proteins, Mater. Lett. 143 (2015) 248–251.
[26] J.C. Lagarias, J.A. Reeds, M.H. Wright, P.E. Wright, Convergence properties of the Nelder-Mead simplex method in low dimensions, SIAM J. Optim. 9 (1998) 112–147.
[27] H. K. Boparai, M Joseph, D. M. O'Carroll, Kinetics and thermodynamics of cadmium ion removal by adsorption onto nano zerovalent iron particles. *J. Hazard. Mater.* 186 (2011) 458–465.
[28] S.W. Nahm, W.G. Shim, Y.K. Park, S.C. Kim, Thermal and chemical regeneration of spent activated carbon and its adsorption property for toluene, Chem. Eng. J. 210 (2012) 500–509.
[29] P.L. Ritger, N.A. Peppas, A simple equation for description of solute release I. Fickian and non-fickian release from non-swellable devices in the form of slabs, spheres, cylinders or discs, J. Control. Release. 5 (1987) 23–36.
[30] P.L. Ritger, N.A. Peppas, A simple equation for description of solute release. II. Fickian and anomalous release from swellable devices, J. Control. Release. 5 (1987) 37–42.
[31] B. Singh, N. Sharma, Development of novel hydrogels by functionalization of sterculia gum for use in anti-ulcer drug delivery, Carbohydr. Polym. 74 (2008) 489–497.